# Chemical mixing in the bottom boundary layer of a eutrophic reservoir: The effects of internal seiching on nitrogen dynamics

**Bridget R. Deemer,\* Stephen M. Henderson, John A. Harrison**
Washington State University Vancouver, School of the Environment, Vancouver, Washington

## Abstract

In lakes and reservoirs, the bottom boundary layer (BBL) mediates chemical fluxes between sediments and the overlying water column. At the internal shoreline, where the thermocline contacts the lakebed, the motions of internal waves can create fluctuating redox conditions and dynamic physical forcing that may support ecologically important reactions such as denitrification. We characterized physical and chemical dynamics within the internal shoreline of a eutrophic reservoir during the spring and early summer of 2012 (18 May to 18 July). An internal seiche was found to generate quasi-periodic fluctuations (periods about 12–24 h) in BBL stratification, temperature, and redox conditions. To examine possible implications for chemical mixing and microbial processing, differences between vertically offset, simultaneous BBL measurements of velocity, temperature, $N_2$, and $N_2O$ were made over 23 h. Vertical differences in BBL temperature, $N_2$, and $N_2O$ formed and collapsed during the wave cycle, with the largest differences occurring following the arrival of an internal bore. Through much of the wave cycle, chemical differences were explained by physical advection and mixing. However, chemical differences measured after bore arrival were not explained by advection, possibly owing to local production of $N_2$ and $N_2O$. These results highlight the dynamic physical environment within the internal shoreline, and the potential of this zone to contribute to system wide denitrification and nitrous oxide production.

In lakes, the bottom boundary layer (BBL) functions as a chemical and physical interface between sediments and the water column (Imberger 1998). The BBL can be defined as the zone immediately above the lakebed where flows are strongly damped by turbulent friction between the water column and sediments. This zone mediates the exchange of solutes and particles between the water column and the sediment (Lorke et al. 2003) and is often a region of sharp redox gradients (Bryant et al. 2010). Mixing across the BBL may, thus, bring substrates, limiting reactants, and microbes together, facilitating important biogeochemical reactions. One process that often relies on mixing of limiting reactants is denitrification, defined here as the microbially mediated conversion of biologically available nitrogen (N) to nonreactive dinitrogen ($N_2$). Denitrification requires suboxic conditions ($< 6.25$ $\mu$mol $O_2$ $L^{-1}$) and reduced electron donors (often organic carbon) to proceed, but also requires oxidized forms of N (e.g., $NO_3^-$), which are produced in an oxygenated environment (Seitzinger et al. 2006). Thus, the transport of water column $NO_3^-$ across the BBL may fuel denitrification in reducing, carbon rich sediments.

Denitrification is an important, but difficult to measure, pathway for N removal in aquatic ecosystems (Groffman et al. 2006; Seitzinger et al. 2006). Previous work to characterize spatial distribution of denitrification in lakes and reservoirs has focused on comparing littoral vs. profundal environments (Saunders and Kalff 2001; David et al. 2006) and on the water column distribution of $N_2$, the end product of denitrification (Deemer et al. 2011; Grantz et al. 2012; Beaulieu et al. 2014). Between littoral and profundal environments lies the internal shoreline, where the thermocline meets the lakebed. This region may be a particularly active site for denitrification and other redox reactions, but we are unaware of any field studies that focus specifically on internal shoreline N dynamics. At the internal shoreline, internal waves (often dominated by energetic internal seiches) can periodically expose the sediments to warm, oxygenated, epilimnetic water followed by cold, hypoxic (or anoxic) hypolimnion water (Fig. 1a–c). In addition to creating a dynamic biochemical environment, internal waves may influence physical mixing of limiting reactants by generating free

*Correspondence: bridget.deemer@email.wsu.edu
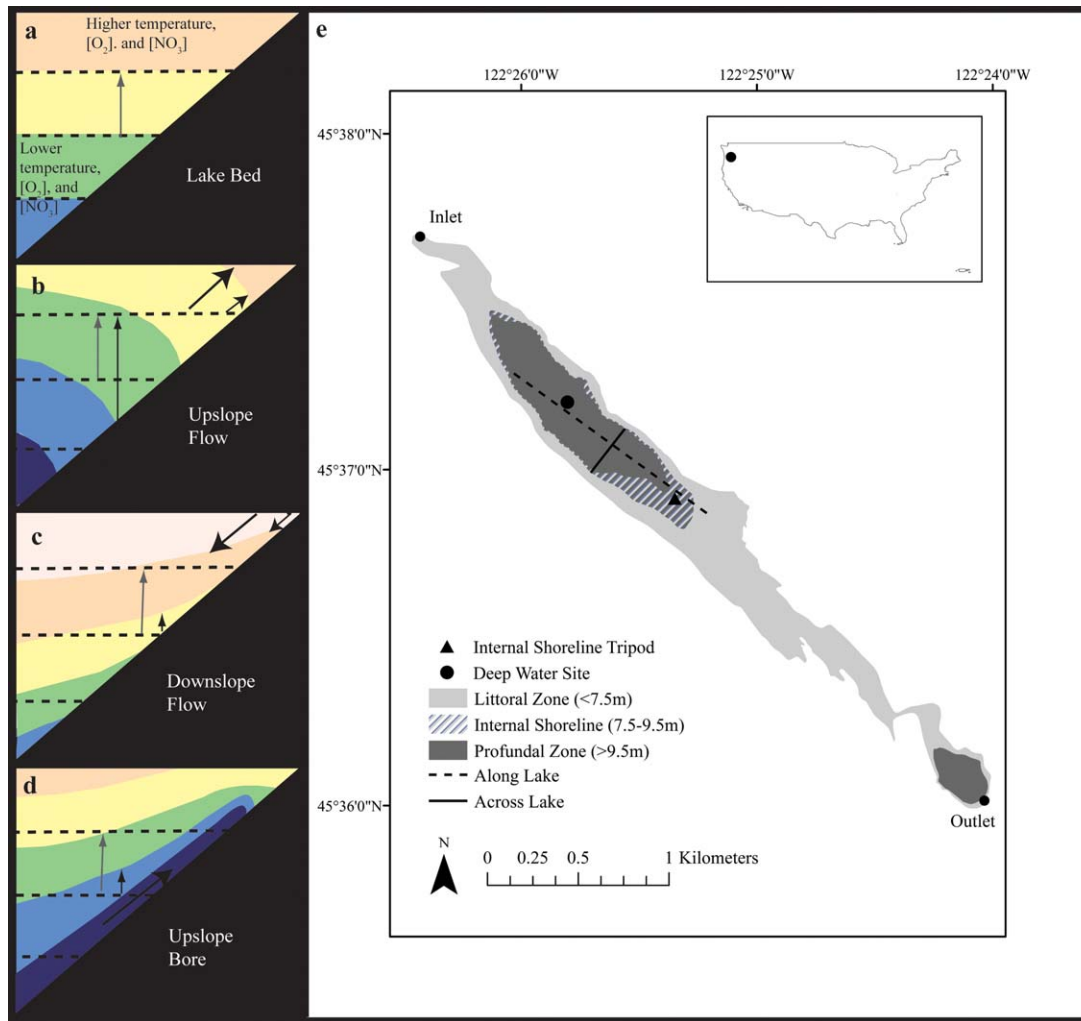
**Fig. 1.** (a–d) Cross-sections of the internal shoreline bottom boundary layer. Contour lines depict thermal stratification and associated chemical stratification during neutral flow (a), upslope flow (b), downslope flow (c), and in the presence of a thin internal bore (d). Near-bed stratification is reduced during upslope flow (b) and intensifies during downslope flow (c) relative to the stratification during neutral flow (a). Dotted lines and grey arrows in panels a-d indicate stratification contours during neutral flow; vertical black arrows in panels b-d show shear induced stratification contours; diagonal black arrows in panels b-d show direction of flow. Study site map (e) showing the locations of the internal shoreline tripod (▲) and deep-water (●) sampling station, as well as the profundal, littoral, and internal shoreline zones of Lacamas Lake. Black dot on insert map indicates the location of Lacamas Lake in Washington State.

convection within sediments (Kirillin et al. 2009), by modifying the thin near-bed diffusive boundary layer (Bryant et al. 2010), or by modifying stratification and mixing in the overlying turbulent BBL.

Internal waves can have a particularly strong influence on BBL stratification and mixing through the process of shear-induced periodic stratification, which occurs when vertically sheared up and downslope flows cause differential advection of stratified waters (Fig. 1a–c, Taylor 1993; Lorke et al. 2005; Umlauf and Burchard 2011; Cossu and Wells 2014). During upslope flow, faster velocities higher above the bed can tilt, or even overturn near-bed isotherms (Fig. 1b), generating weak or reversed stratification and relatively intense turbulence

(Lorke et al. 2005). Conversely, during downslope flow lighter fluid can be preferentially advected over denser fluid (Fig. 1c), enhancing stratification, and inhibiting turbulence (Lorke et al. 2005).

The simple pattern of shear-induced periodic stratification, outlined above, can be complicated by stepwise transitions from down- to up-slope flow associated with the arrival of "internal bores" (Fig. 1d). These bores form as closely spaced isotherms at the leading edge of a cold-water layer propagate up the lakebed and pitch forward within the BBL, in a manner reminiscent of breaking surface waves. Theoretical models predict that bore development might be particularly effective when the bed slope nearly equals the slope of

internal wave "characteristic curves" (i.e., the curves along which wave energy propagates). However, near-equality of bed and characteristic slopes is not essential to bore formation. Instead, weakly nonlinear perturbation expansions show that bores may be widespread when isotherm tilt becomes comparable to bed slope (Thorpe 1992, 1999). Observations confirm that bores are commonly observed near sloping beds in lakes (Thorpe and Lemmin 1999; Cossu and Wells 2014) and in a wide range of oceanic environments (Winant 1974; Bluteau et al. 2011; Walter et al. 2014). Sufficiently near the bed, bore arrival and the associated transition to upslope flow is expected to reduce stratification, but the zone of reduced stratification can be very thin. For bores that are thinner than the scale over which BBL stratification is measured, the transition to upslope flow is associated with increased BBL stratification (Fig. 1d), in contrast to the decreased stratification that would typically accompany upslope flow (Fig. 1b).

Here, we focus on the interactions between water flows, stratification and vertical differences in chemical concentrations within the BBL. Vertical differences in BBL chemical concentrations are of particular interest owing to their potential to shed light on chemical fluxes at the sediment water interface (Holtappels et al. 2011). For example, elevated near-bed $N_2$ concentrations within the BBL may provide evidence for sediment-based denitrification and associated $N_2$ production. In the coastal ocean, BBL chemical gradients have been attributed to biogeochemical fluxes, leading to quantitative flux estimates (Holtappels et al. 2011; McGillis et al. 2011). For lakes, based on previous observations of strong shear-induced periodic temperature stratification, we hypothesize that BBL chemical gradients induced by local biogeochemical processing can be modified by physical advection. Specifically, sheared BBL velocities might generate larger vertical $N_2$ concentration differences during stratified downslope flow (Fig. 1c), and smaller vertical $N_2$ concentration differences during less stratified upslope flow (Fig. 1b), with this trend possibly complicated by the arrival of thin internal bores (Fig. 1d). Identification of such advection-induced concentration differences is required for proper interpretation of BBL chemical concentration differences; only after advective concentration differences are removed can residual concentration differences be used to shed light on local biogeochemical processing.

The aim of this study was to identify the role of physical advection in the formation of vertical chemical differences within the BBL. To do this, we measured the vertical offset in temperature, velocity, and nitrogenous solute concentrations within the internal shoreline of a small eutrophic reservoir over a 23-h wave cycle. Vertical differences in BBL chemistry induced by physical advection were estimated using measured BBL temperature differences and relationships between temperature and nitrogenous solutes observed at the deepest site within the reservoir. The relative importance of advection was then quantified by comparing measured chemical differences with the estimated advection-based vertical differences. We also estimated the residual difference in nitrogenous solutes that could not be explained by physical advection. It is this residual difference that has potential to shed light on microbial N cycling. Patterns in the formation and collapse of temperature and chemical stratification within the BBL were placed into the context of a longer 62-d deployment of velocity and temperature sensors at the same site that spanned the 23-h intensive sampling. This longer term dataset supported a better characterization of internal wave dynamics within the BBL and, together with background $O_2$ concentrations, an analysis of the physiochemical conditions under which residual nitrogenous chemical differences were observed.

## Methods

### Study site

Lacamas Lake is a small ($1.3\,km^2$), long, narrow reservoir in southwest Washington State (45.37N, 122.25W, Fig. 1e). It has an average depth of $7.8\,m$ and a maximum depth of $19.8\,m$. A dam was built in 1938, deepening the preexisting lake, and it is currently operated primarily for recreational purposes. Lacamas Lake experiences strong thermal stratification from early June to October, with a thermocline between $4\,m$ and $7\,m$ depth. The reservoir is eutrophic and complete hypolimnetic hypoxia is generally observed within weeks of the onset of stratification (Deemer et al. 2011). Velocities are dominated by a seiche-like, wind-driven internal wave with a horizontal wavelength that exceeds the metalimnion length and a period of between $12\,h$ and $24\,h$ (Henderson and Deemer 2012). This internal wave propagates vertically carrying energy to the lakebed (Henderson and Deemer 2012), and causes the depth of the thermocline to oscillate up to $2\,m$ at the internal shoreline. The southeast region of the internal shoreline (where the thermocline meets the lakebed) is broad and gradually sloped creating a relatively large internal shoreline region (Fig. 1e).

### BBL chemical measurements

To shed light on chemical mixing in the bottom boundary layer, 74 pairs of $N_2$ : Ar samples, 37 pairs of $N_2O$ samples, and 9 pairs of grab samples for $NO_3^-$ and $NH_4^+$ were obtained between 10:00 h PST 15 June 2012 and 09:00 h 16 June 2012. The $N_2$ : Ar samples were collated into 11 sets, roughly one for every 2 h of sampling, and $N_2O$ samples were collated into 10 sets. Two narrow gauge silicon tubes (1/8″ ID) were attached to a large (1.5 m tall) aluminum tripod in 8.5 m water depth to obtain paired samples from elevations $z = 0.1\,m$ and $0.4\,m$ above the bed, within the internal shoreline (Internal Shoreline Tripod Site, Fig. 1e). Samples were manually pulled up from depth at a rate of approximately $1\,mL\,s^{-1}$ using $60\,mL$ BD luer lok syringes. Samples were used to flush and fill Labco exetainers (for $N_2$ : Ar analysis), small aluminum crimp-top wheaton vials (for $N_2O$ analysis), or were filtered into $30\,mL$

plastic HDPE Nalgene bottles (for nutrient analysis). To estimate vertical concentration differences, paired samples at $z = 0.1$ m and 0.4 m, collected within 5 min of each other, were differenced to obtain between 3 and 9 concentration difference estimates for each measurement set. Samples that failed to meet QA/QC criteria (see below section on MIMS) or that contained bubbles were omitted from the analysis.

## Physical measurements

Physical measurements were collected from a single site within the internal shoreline (Internal Shoreline Tripod Site; Fig. 1e) between 18 May 2012 and 18 July 2012. Boundary layer water velocity profiles were measured using a 2 MHz Nortek Aquadopp Acoustic Doppler Profiler (ADP) mounted on the large tripod described above. The ADP was mounted at elevation $z \approx 1.3$ m above the bed, and pointed downward to measure velocity every 0.015 m from $z = 0.135$ m to $z = 1.14$ m. At $z < 0.135$ m, velocities may have been contaminated by acoustic sidelobe reflections from the bed, and were discarded. The ADP operated in pulse-coherent mode (Lohrmann et al. 1990), recording one 1-s burst of two 2-Hz measurements every 12 s throughout the 62 d deployment. Water column temperatures were measured using four RBR loggers attached to the main lander at $z = 0.2$ m and 0.4 m (fast-response RBR TR-1060s, logging every 2 s), and at $z = 0.9$ m and 1.3 m (RBR XR-420 CTs, logging every 10 s). Owing to the small depth range, adiabatic temperature corrections did not significantly affect estimates of density stratification, and were neglected.

The 62 d of ADP and temperature data were divided into hourly segments. ADP measurements associated with acoustic correlations $< 90\%$ were discarded (Rusello 2009). Hourly means were used for all results presented below, except those shown in Fig. 5. Standard coordinate transformations, and measured instrument heading, pitch, and roll, were used to convert hourly mean ADP along-beam velocities into eastward, northward, and upward coordinates. The "along-lake" coordinate, 126° clockwise from North (dashed line, Fig. 1e), was chosen as the principle axis of the covariance matrix between hourly averaged ADP eastward and northward velocities measured 0.3 m above the bed.

## Water column chemistry

$N_2 : Ar$, $N_2O$, $NO_3^-$, and $NH_4^+$ samples were collected with a Van Dorn sampler from the deepest part of the reservoir (Deep-Water Site; Fig. 1e) on five dates between 30 May 2012 and 26 July 2012 at 0.1, 1, 2, 4, 5.5, 7, 9, 11, 13, and 15 m depth as well as 0.2 m off the lakebed. Either a Hach DS5X Sonde or an In Situ Troll 9500 was used to measure temperature and dissolved oxygen at each sampling depth.

To characterize $O_2$ dynamics within the internal shoreline, an In Situ Troll 9500 equipped with a temperature probe and optical dissolved oxygen sensor was deployed within 10 m of the large tripod (Internal Shoreline Tripod Site; Fig. 1e) on two separate occasions during the spring of 2012. The Troll 9500 was attached to a second, smaller

(0.5 m × 0.5 m) aluminum lander 0.1 m above the lakebed and logged at 15 min intervals during the first deployment and at 2 min intervals during the second deployment. The first Troll 9500 deployment occurred from 16 May 2012 at 16:00 h to 30 May 2012 at 13:30 h. The second deployment coincided with the 24-h sampling described above and lasted from 11:15 h on 15 June 2012 to 10:00 h on 16 June 2012.

## Laboratory analysis

For analysis of $NO_3^-$ and $NH_4^+$, filtered (Whatman GF/F 0.45 $\mu$m) water samples were collected in acid-washed 30 mL plastic HDPE Nalgene bottles and stored frozen until analysis on a Westco discrete nutrient analyzer using standard EPA-approved colorimetric methods (method number 353.2 for $NO_3^-$ and 4500-NH$_3$-G for $NH_4^+$, National Environmental Methods Index, www.nemi.gov). The detection limits were 0.4 $\mu$mol L$^{-1}$ for $NO_3^-$ and 0.6 $\mu$mol L$^{-1}$ for $NH_4^+$.

Water column $N_2O$ samples were collected in 72 mL crimp-top Wheaton vials, treated with saturated $ZnCl_2$ to stop microbial activity, and analyzed using a gas equilibration technique as in Harrison and Matson (2003). Briefly, samples were brought to 25 °C, and 20 mL of ultrahigh purity helium headspace was introduced to Wheaton vials. Following headspace introduction, vials equilibrated for at least 24 h before headspace gas was analyzed using a Hewlett Packard 5890 Series II Plus gas chromatograph equipped with an electron capture detector (ECD). The ECD contained $^{63}$Ni as the isotope source, and a mixture of argon and methane was used as the carrier gas as in Harrison and Matson (2003). Every six samples, 0.1 ppm and 5 ppm $N_2O$ standards were run. Coefficient of determination ($R^2$) values for calibration curves were never lower than 0.98 using repeated measurements of $N_2O$ at each standard concentration, and the mean percent coefficient of variation of standards (defined as 100 × SD/Mean where SD is the standard deviation of standard concentration readings from a single run, and Mean is the mean standard concentration reading from a single run) was 8.7%. Headspace $N_2O$ concentrations were converted to original dissolved gas concentrations using the appropriate solubility tables (Weiss and Price 1980). Expected $N_2O$ concentrations were then calculated based on the sample collection temperature and established temperature solubility rules (Weiss and Price 1980). $N_2O$ in excess of saturation is reported as "excess" $N_2O$ and is considered the result of microbial activity.

$N_2 : Ar$ and $O_2 : Ar$ samples were collected in duplicate 12 mL Labco exetainers, treated with $ZnCl_2$, and refrigerated under water prior to analysis for $N_2 : Ar$ ratios on a Membrane Inlet Mass Spectrometer (MIMS) as in Kana et al. (1994). Samples were run within 98 d of collection and there was no detectable effect of the time elapsed between sample collection and analysis on measured $N_2$ ($p \gg 0.05$ for a regression of time vs. $N_2 : Ar$). Laboratory procedures and calculations of excess $N_2$ are described in Deemer et al. (2011). Briefly, five readings were taken from each sample vial to record the ratio of atomic

mass (AM) 28 and 40 signals. Percent coefficient of variation for replicate readings from the same sample had to be $< 0.05\%$ for the instrument to be considered stable. Three temperature standards verified linearity of the raw signals of $N_2$, Ar, and $N_2$ : Ar across the range of $[N_2]$, $[Ar]$, and $N_2$ : Ar measured in this study. Deionized water (air-equilibrated at 24–25 °C) was then run as a standard every six samples, and repeat standards were used to correct for instrument drift. The mean percent coefficient of variation between replicate standard readings was 0.025% (SD 0.012). The expected $N_2$ : Ar ratio of each sample was calculated based on the sample collection temperature and solubility tables developed by Weiss (1970). These expected ratios were compared to measured drift-corrected $N_2$ : Ar ratios under the assumption that $[Ar]$ varied only due to physical factors (e.g., temperature), while $[N_2]$ varied due to both physical and biological factors. Total $N_2$ concentrations were then quantified for all the samples collected as:

$$\text{Total } N_2 = \frac{N_2 : Ar_{\text{measured}}}{N_2 : Ar_{\text{expected}}} * N_{2\,\text{expected}} \qquad (1)$$

where $N_2 : Ar_{\text{measured}}$ is the drift corrected $N_2$ : Ar ratio, and $N_2 : Ar_{\text{expected}}$ and $N_{2\,\text{expected}}$ are the atmospheric-equilibration-based $N_2$ : Ar ratio and $[N_2]$, respectively, which are quantified based on the temperature specific solubility of $N_2$ and Ar. Patterns in deep water excess $[N_2]$ and $[N_2O]$ were also quantified to consider spatial patterns within the water column. $N_2$ in excess of the expected $N_2$ : Ar ratio is reported as excess and is considered a product of denitrification as in Deemer et al. (2011). $N_2O$ in excess of temperature-dependent saturation with the atmosphere is also defined as excess and is considered a product of either nitrification or denitrification as in Deemer et al. (2011).

For both $N_2$ and $N_2O$ sampling, care was taken to avoid gas bubble entrainment, which interferes with sample analysis. For $N_2O$ samples, four samples from 11 July and one sample from 26 July had to be discarded due to improper sealing or bubble formation. For $N_2$ : Ar samples, at least one of two replicate samples at each sampling point remained air bubble-free for all profile samples collected.

### Modeling of advection-based concentration differences

During summer, $N_2$ and $N_2O$ accumulate in the hypolimnion of Lacamas Lake, resulting in $[N_2]$ and $[N_2O]$ that are negatively correlated with temperature at depths intersecting the internal shoreline (Deemer et al. 2011; and Fig. 7 herein). If these relationships hold in the internal shoreline, then vertical differences in shoreline $N_2$ and $N_2O$ concentrations may simply reflect lakewide gradients, modified by local physical advection and mixing, with no need to invoke local $N_2$ or $N_2O$ production. We used temperature as a tracer to investigate the role of physical advection and mixing of background stratification in controlling vertical concentration differences in nitrogenous solutes. We modeled expected advection-based concentrations and resultant differences

using relationships between temperature and solute concentration measured in the deep lake. We first determined relationships between temperature and concentration outside the boundary layer:

$$C_{\text{fit}} = aT + b \qquad (2)$$

where $a$ and $b$ were chosen by linear regression between chemical concentrations and temperatures measured at the deep water site, at 5.5 m, 7 m, 9 m, and 11 m depth, on 19 June. Chemical concentrations at $z = 0.1$ m and 0.4 m within the BBL, denoted $C_{1\text{fit}}$ and $C_{2\text{fit}}$, were then predicted using Eq. 2 and BBL temperatures measured at $z = 0.1$ m and 0.4 m. Now the difference between the observed BBL concentration differences and the difference expected given observed stratification:

$$(C_1 - C_2)_{\text{residual}} = (C_{1\,\text{measured}} - C_{2\,\text{measured}}) - (C_{1\,\text{fit}} - C_{2\,\text{fit}}) \qquad (3)$$

is the component of the boundary layer concentration difference that can not be explained by lakewide advection, and might result from local microbial processing. We refer to this as the residual concentration difference.

### Statistical and error analysis

We performed several sensitivity analyses to determine how individual measurement errors may affect our ability to estimate vertical differences in chemical concentrations. Temperature logger error may affect $N_2$ and $N_2O$ concentration difference calculations because the $N_2$ : Ar and $N_2O$ calculations are temperature dependent. Reported accuracy of RBR temperature loggers is $\pm 0.002$ °C with a drift of less than 0.002 °C yr$^{-1}$. To estimate the potential effect of temperature logger-related error, we quantified the average artificial $N_2$ and $N_2O$ concentration difference that would result from an artificial temperature gradient of 0.008 °C. In addition, the instrument noise floor for both the MIMS and the GC may noticeably affect the precision of the chemical concentration difference estimates. We quantified the perceived concentration difference that would result from overestimating the concentration at 0.1 m and underestimating the concentration at 0.4 m based on the mean instrument coefficient of variation. MIMS measurements of $O_2$ : Ar were not used in this analysis because of high variation in replicate samples from single Van Dorn casts (average of 10% coefficient of variation).

The silicon tubing we used to collect BBL nitrogenous gas samples is somewhat gas-permeable. We used Fick's Law to estimate the exchange between the water column and the tube samples. This exchange, referred to as the diffusive flux, J, has units of mol m$^{-2}$ s$^{-1}$ and was quantified as

$$J = -D \frac{\partial \phi}{\partial x} \qquad (4)$$

where $D$ is the diffusion coefficient in m$^2$ s$^{-1}$, $\partial \phi$ is the concentration difference in mol m$^{-3}$, and $\partial x = 0.00158$ m is the thickness of the tubing. The diffusion coefficient was estimated

using published values for $N_2$ and $N_2O$ in silicone rubber (Robb 1968). $\partial\phi$ was estimated as the difference between the surface water concentration of $N_2$ and $N_2O$ and the concentration measured at 7 m and 9 m. Concentration estimates were taken from the deep water profiles collected on 8 June and 19 June. The change in gas concentration within each sample due to tube permeability, $\Delta g$, was then estimated as

$$\Delta g = \frac{J * \text{SA} * T}{V} \tag{5}$$

where SA is the surface area of the entire inner-layer of the tube in $m^2$ (0.135), $T$ is the time the sample took to travel through the tube in s (64), and $V$ is the volume of water held by the tube in L (0.107).

A laboratory test was conducted to confirm the $N_2$ permeability of our sample tubing. 15.5 m of silicon tubing (identical to the tubing used for field sampling) was immersed in a bucket of deionized water and held at 10 °C overnight. Several liters of additional deionized water were set on a stir plate and allowed to equilibrate at ambient room temperature overnight. The next day, triplicate samples of deionized water were collected from both temperature treatments by overflushing Labco exetainers. The silicon tubing was then used to collect triplicate samples of room temperature water that was drawn through 15 m of tubing immersed in the 10 °C bucket. We also timed the rate at which samples were drawn (to quantify $T$ in Eq. 5 above). All samples were run for $N_2$ : Ar using MIMS and the observed change in $N_2$ concentration ($\Delta$) of room temperature samples that were passed through 10 °C water was used to calculate J and solve for D.

For our statistical analysis, we treat successive concentration difference measurements as uncorrelated, an assumption supported by direct estimation of equivalent degrees of freedom from sample autocorrelation functions (Garrett and Petrie 1981). One-sample, two-tailed *t*-tests were used to assess whether measured and residual $N_2O$ concentration differences were significantly different from zero. One-sample, one-tailed *t*-tests were used to assess whether measured and residual $N_2$ concentration differences during individual measurement periods were significantly larger than zero. One-tailed *t*-tests are appropriate for this analysis (unlike in many other ecological analyses, Lombardi and Hurlbert 2009), because we are concerned with identifying positive (bed-elevated) concentration differences, which are consistent with $N_2$ production. We did not interpret negative concentration differences any differently from statistically insignificant positive concentration differences (Ruxton and Neuhäuser 2010). This follows from a fundamental assumption (that is consistent with our observations), that $N_2$ fixation is not an important processes at 8.5 m water depth (Deemer et al. 2011).

Linear relationships between temperature and both $N_2$ and $N_2O$ were fitted using least squares regression. For all the parametric tests described above, data were first tested to ensure they met assumptions of equal variance and normal
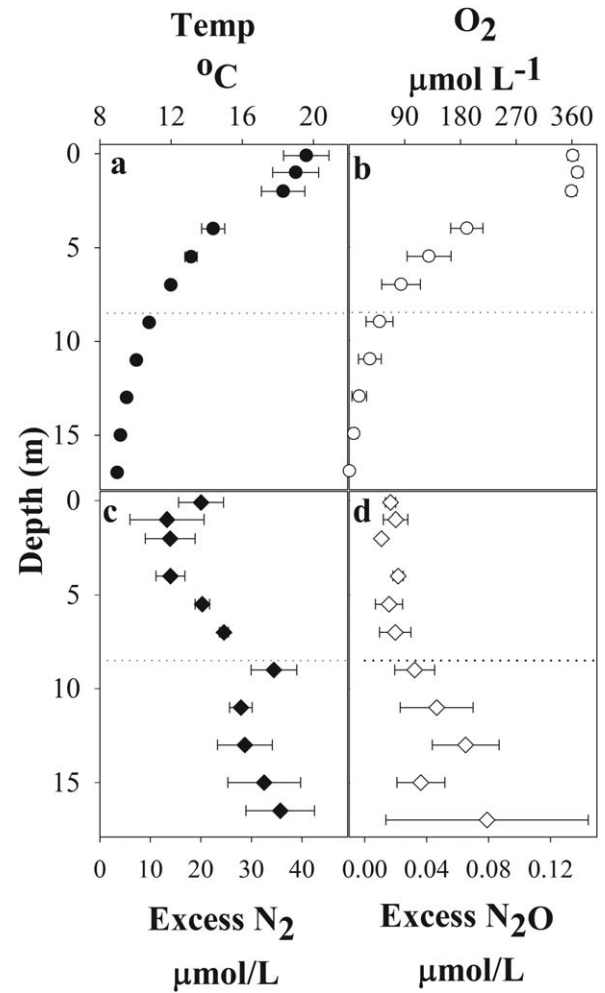


**Fig. 2.** Average profiles of temperature (a), dissolved $O_2$ (b), excess $N_2$ (c), and excess $N_2O$ (d) at the deep water site between 30 May and 26 July. The dotted line indicates the depth of the internal shoreline tripod. Standard error bars shown ($n = 5$).

distribution. All statistical tests were performed using R version 3.1.1 and alpha was set at 0.05.

Based on the lack of measureable autocorrelation, we estimated the standard deviation of the 23-h sample-mean chemical concentration difference, denoted std($G$), as

$$\text{std}(G) = \sqrt{\frac{\sum_{j=1}^{N} \sigma_j^2}{N}} \tag{6}$$

where $N$ = number of measurement periods, and $\sigma_j$ is the standard error of concentration differences determined from paired measurements within period $j$. Since mean chemical concentration differences were calculated from a large number of observations (74 for $N_2$ and 37 for $N_2O$), significance can be determined using a $Z$ test for the ratio between the estimated mean concentration difference and std($G$).
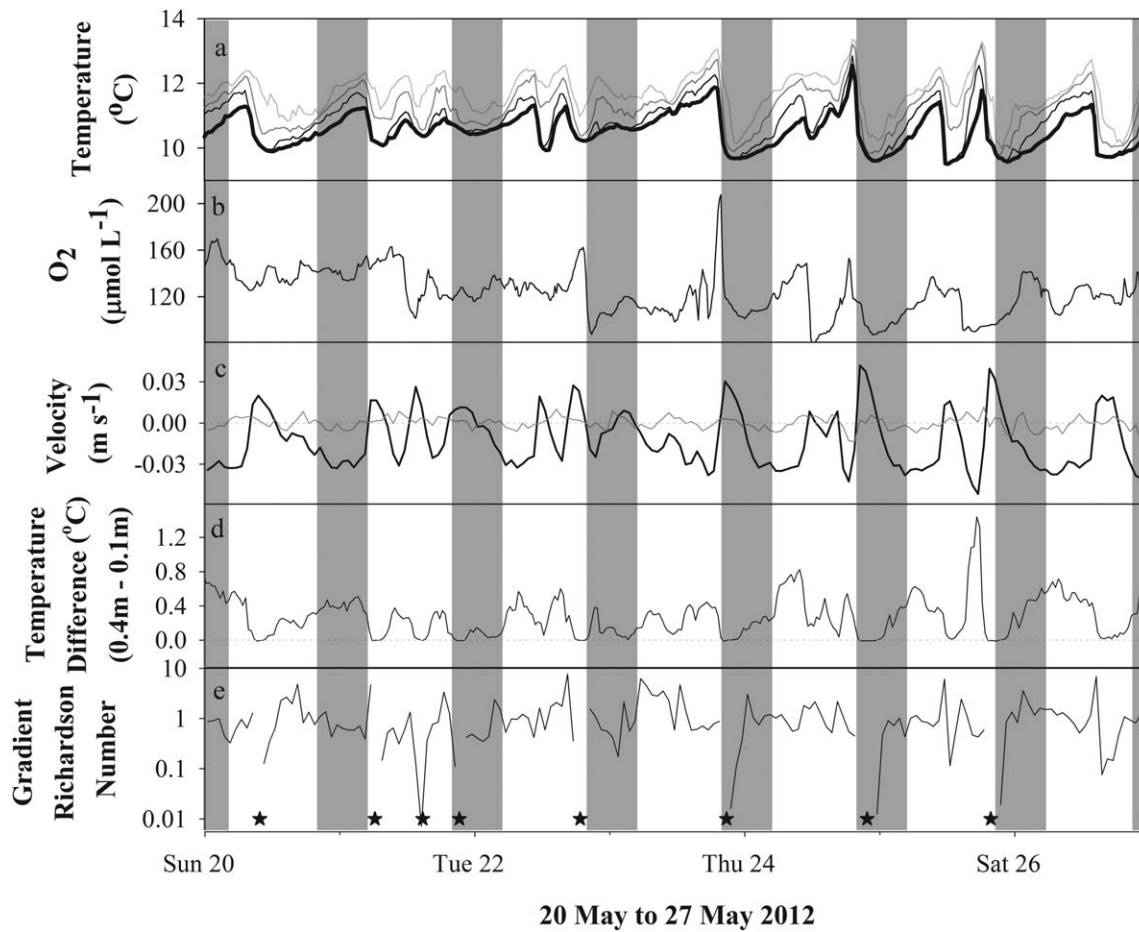
**Fig. 3.** Temperature measured at $z = 0.2$, 0.4, 0.9, and 1.3 m from darkest line to lightest line, respectively (a), dissolved oxygen measured at $z = 0.1$ m (b), hourly mean along and across lake velocities (along lake velocity in black and across lake velocity in gray, (c), temperature difference between $z = 0.4$ m and $z = 0.1$ m (d), and gradient Richardson numbers (e) within the bottom boundary layer between 20 May 2012 and 27 May 2012. Gray bars represent the period from sunset to sunrise. Positive velocity values indicate upslope flow for along-lake velocities and flow toward the northeast for across-lake velocities. Unstable stratification events are marked by stars in panel (e), and associated gradient Richardson numbers are not plotted due to log scale.

## Results

Deep water profiles in Lacamas Lake showed strong thermal and chemical stratification (Fig. 2). Strong fluctuations in both physical and chemical parameters were observed at the internal shoreline of Lacamas Lake (Fig. 3). Temperature fluctuations exceeding 2 °C and $O_2$ fluctuations exceeding 60 $\mu$mol L$^{-1}$ were routinely observed over single wave periods. These fluctuations, together with fluctuations in near-bed stratification (Fig. 4) were largely synchronized with along lake velocity. During the 23-h sampling period, significant BBL chemical concentration differences were mainly observed during the first half of the sampling event and followed the arrival of a thin internal bore (Figs. 5, 6). Collapse of chemical concentration differences coincided with collapse of temperature stratification (Fig. 6). Vertical differences in nitrogenous gas concentrations were largely explained by fluctuations in BBL temperature stratification, but significant residual
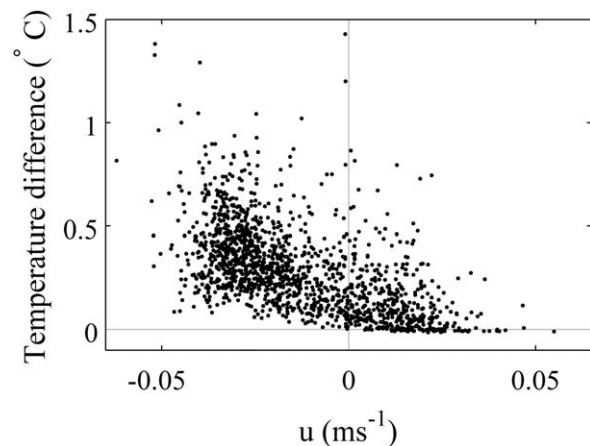


**Fig. 4.** Stratification (temperature 0.4 m above bed minus temperature 0.1 m above bed) vs. upslope water velocity. Each data point is a 1 h average, all 1430 h of good data shown.
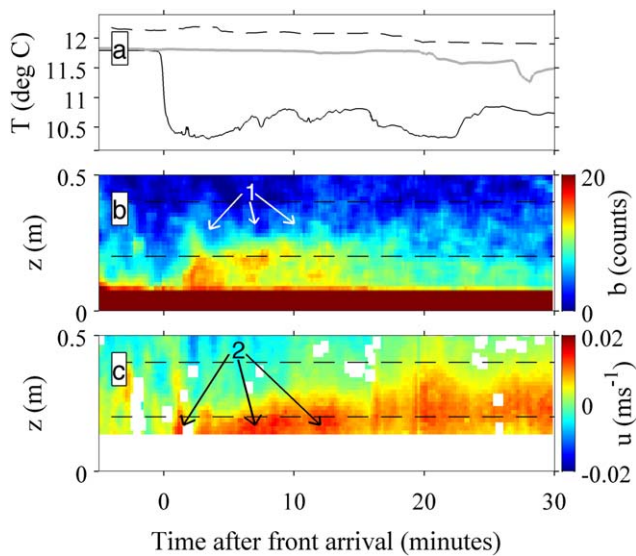
**Fig. 5.** Arrival of a thin bore. Panel a: Temperature measured 0.1, 0.4, and 0.9 m above the bed (respectively thin black, thick gray, and dashed lines). Panel b: acoustic backscatter b, with trends resulting from beam spreading and attenuation removed. Panel c: upslope water velocity. Horizontal dashed lines in panels b and c indicate elevations of temperature gauges. The arrival of the thin bore (marked by sudden near-bed temperature drop, panel a), was followed by elevated near-bed backscatter (labeled 1 in panel b), and slow upslope water velocity within 0.2 m of the lakebed (labeled 2 in panel c).

concentration differences were also detected. The largest residual $N_2$ difference coincided with the lowest BBL $O_2$ concentrations, whereas the largest residual $N_2O$ differences coincided with low-to-intermediate $O_2$ concentrations.

**Lakewide physiochemical environment**

Lacamas Lake was thermally stratified for the duration of this study and the internal shoreline tripod was located below the metalimnion (Fig. 2a,b). Surface waters were approximately 10 °C warmer than bottom waters (average of 19.59 °C and 8.98 °C, respectively) and oxygen conditions ranged from supersaturation in the surface water to anoxic conditions in the bottom water (average of 132% and 0.2% $O_2$, respectively). Excess $N_2$ and $N_2O$ were elevated in bottom waters relative to surface waters (Fig. 2c,d) and a peak in excess $[N_2]$ was observed at 9 m depth, close to the depth of the internal shoreline tripod (Fig. 2c).

At the internal shoreline, hourly water temperature, velocity, and $O_2$ concentration fluctuated quasi-periodically, with dominant periods about 12–24 h (Fig. 3a–c). ADP-measured along-lake water velocities (u) dominated over across-lake velocities (v) (Fig. 3c). Throughout the 62 d deployment, root-mean-square along- and across-lake velocities were $0.024\ ms^{-1}$ and $0.005\ ms^{-1}$, respectively (unless specified otherwise, velocities presented were measured at $z = 0.3$ m). Temperature and dissolved oxygen fluctuations were not synchronized with periods of sunlight or darkness (white and gray regions, Fig.

3a,b), but instead followed velocity fluctuations (compare Fig. 3a,c). These velocity fluctuations are caused by a lakewide internal wave, likely forced by daily wind fluctuations associated with the nearby Columbia River Gorge (Henderson and Deemer 2012). Coherence of 70% between internal shoreline measurements and thermistor measurements made at the other end of the lake confirm the role of lake wide internal waves in dominating these fluctuations (Henderson unpubl.).

Internal shoreline fluctuations in temperature and thermal stratification were qualitatively consistent with advection and tilting of isotherms by sheared up- and down-slope flows (Fig. 1a–c). Downslope flows were generally associated with increasing temperature and oxygen content, whereas pulses of upslope flows were associated with rapid drops in temperature and dissolved oxygen (compare Fig. 3c with
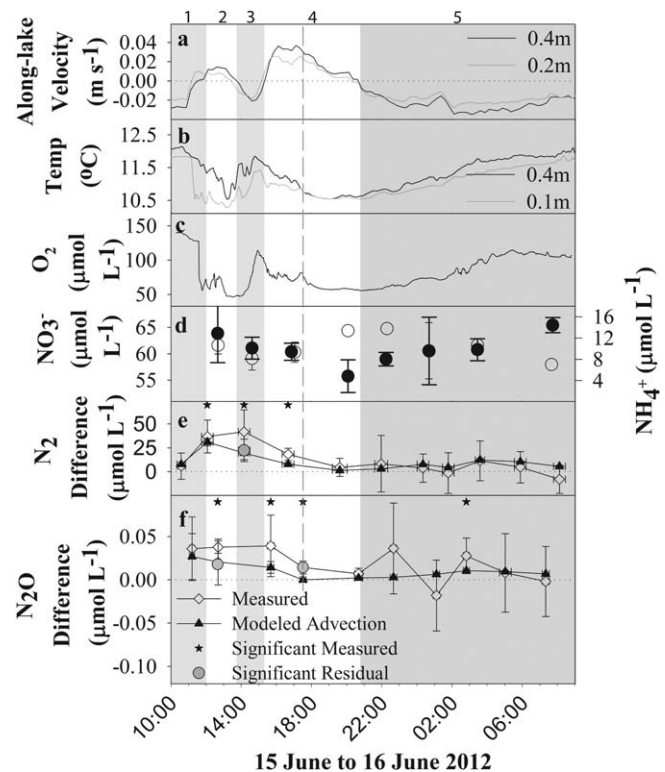


**Fig. 6.** Along-lake velocity (positive values indicate upslope flow, (a), temperature (b), dissolved oxygen concentrations at $z = 0.1$ m (c), mean $NO_3^-$ (hollow circles) and $NH_4^+$ (black circles) concentrations (d), $N_2$ concentration differences (e), and $N_2O$ concentrations differences (f) within the BBL over a 23 h wave period. In (e) and (f), hollow diamonds show total measured concentration differences whereas black triangles show the advection-based concentration differences based on temperature modeling. Black stars indicate measured concentration differences that were statistically different from zero (one sample *t*-test, $p < 0.05$). Gray circles show significant residual concentration differences (where measured and modeled vertical concentration difference were significantly different by *t*-test, $p < 0.05$). Gray dashed line demarcates the collapse in BBL thermal stratification. Five subintervals are also specified at the top of the figure: (1) arrival of thin bore, (2) sheared upslope flow, (3) small shear and no trend in stratification, (4) strongly sheared upslope flow, and (5) downslope flow. 95% confidence intervals shown.

3a,b). Flows were typically slower nearer to the bed, resulting in more stratified conditions during downslope flow and less stratified conditions during upslope flow (Fig. 4), consistent with our conceptual model (Fig. 1b,c). Cases of measureable unstable stratification were rare (19 of 1430 h), but all occurred during upslope flow (Fig. 3d). Unstable stratification events were always small (see negative temperature differences in Fig. 4). Although trends were consistent with the conceptual model of Fig. 1a–c, scatter about these trends was substantial (Fig. 4). More complex relationships between velocity and stratification were examined, but did not reduce scatter (approaches tested included allowing for a time-lagged response of stratification to velocity, and relating stratification to the shear, or to time-integrated shear).

Internal bores can explain some of the observed scatter in the relationship between velocity and stratification. Each internal bore was characterized by a sudden drop in near-bed temperature, a simultaneous change in near-bed acoustic backscatter intensity, a stepwise transition to upslope near-bed flow, and a pulse of flow away from the bed. During the entire 62 day study period, we observed 13 distinct bores with heights between 0.4 m and 0.9 m, all associated with temperature drops of more than a degree in less than 30 s and rapid transitions to upslope flows (on the order of a few cm s$^{-1}$) at $z = 0.1$ m and 0.4 m. Two cases of bores with heights exceeding 0.9 m were observed, identified by transition to upslope flow throughout the bore and nearly simultaneous stepwise temperature drops at $z = 0.1$ m, 0.4 m, and 0.9 m. Five additional cases were observed where stepwise temperature drops at $z = 0.1$ m were not followed by stepwise drops at $z = 0.4$ m. These cases were interpreted as bores with heights $< 0.4$ m. A particularly thin and weakly developed bore arrived during the 23-h chemical sampling event at 11:15 h on 16 June, when a near-bed temperature drop of 1.4 °C (Fig. 5a) was followed by elevated near-bed backscatter (labeled 1 in Fig. 5b), and slow upslope water velocity within 0.2 m of the lakebed (labeled 2 in Fig. 5c). A pulse of upward velocity was observed immediately following the arrival of the bore (not shown), indicating that warmer water was pushed up over the advancing thin, cold layer (time integration of the velocity pulse yielded an upward displacement of about 0.3 m).

An important measure of the ability of stratification to inhibit vertical turbulent mixing is the dimensionless gradient Richardson number

$$Ri = \frac{g(\rho_2 - \rho_1)(z_2 - z_1)}{\rho_1[(u_2 - u_1)^2 + (v_2 - v_1)^2]} \tag{7}$$

Here $\rho$ is the hourly mean water density, calculated from temperature, and subscripts 1 and 2 indicate variables measured at elevations $z_1 = 0.2$ m and $z_2 = 0.4$ m. Owing to strong near-bed stratification, the gradient Richardson number often exceeded 0.25 (Fig. 3d). Such high Richardson numbers

indicate that stratification was often sufficiently strong to inhibit BBL turbulence and mixing (Monin and Yaglom, 1975). In contrast, the few unstable stratification events mentioned above were associated with small Richardson numbers.

**Physiochemical dynamics during 23-h sampling event**

The period of intensive chemical sampling captured approximately one complete wave cycle, with two punctuated periods of upslope flow during the first half of the wave cycle, followed by a prolonged period of downslope flow during the second half (Fig. 6a). We distinguish five subintervals during the period of intensive sampling (Fig. 6). Development of stratification during subinterval 1 was dominated by the arrival of a thin near-bed bore (shown in detail in Fig. 5, and described above). During subinterval 2, sheared upslope flow was associated with weakening stratification, as expected (as in conceptual diagram, Fig. 1b). During subinterval 3, shear was small (black and gray lines in Fig. 6 a lay on top of each other) and there was no clear trend in stratification. During subinterval 4, strongly sheared upslope flow developed, and as expected (Fig. 1b) stratification was reduced and eventually eliminated. During the final interval, interval 5, downslope flow developed, together with steadily increasing stratification as expected (as in conceptual diagram, Fig. 1c).

Clear near-bed temperature stratification was observed during most of the period of intensive chemical sampling (temperature averaged 0.27 °C warmer at 0.4 m off the bed than at 0.1 m off the bed), with the exception of 18:00 h–19:00 h, when water became essentially unstratified (Fig. 6b). The collapse in thermal stratification coincided with strong upslope flow (Fig. 6a) and the arrival of colder, oxygen-depleted water (Fig. 6c). Along-lake velocities were particularly strongly sheared during this time (compare black and gray lines of Fig. 6a), likely promoting the loss of stratification.

**Vertical differences in chemistry during the 23-h sampling event**

Variable but significant near-bed concentration differences in $N_2$ and $N_2O$ were observed in the internal shoreline with the passing of the internal wave (Fig. 6e,f). In the case of $N_2$, the largest concentration differences occurred after the arrival of the thin bore and prior to the collapse in thermal stratification (compare Fig. 6b,e). In 55 of 74 sample pairs, $N_2$ concentrations 0.1 m above the bed exceeded concentrations 0.4 m above the bed, and all three significantly nonzero measurement sets had positive (i.e., bed-elevated) differences (one sample $t$-test with $p < 0.05$, Fig. 6e). $N_2$ averaged 11.4 $\mu$mol $N_2$ L$^{-1}$ higher at 0.1 m off the bed than at 0.4 m off the bed (Std$(G) = 2.8$ $\mu$mol $N_2$ L$^{-1}$, $Z$-score = 4.1). For 32 of 37 sample pairs, $N_2O$ concentrations were elevated near the bed, and there were three sets of significantly bed-elevated concentrations (one sample $t$-test with $p < 0.05$, Fig.
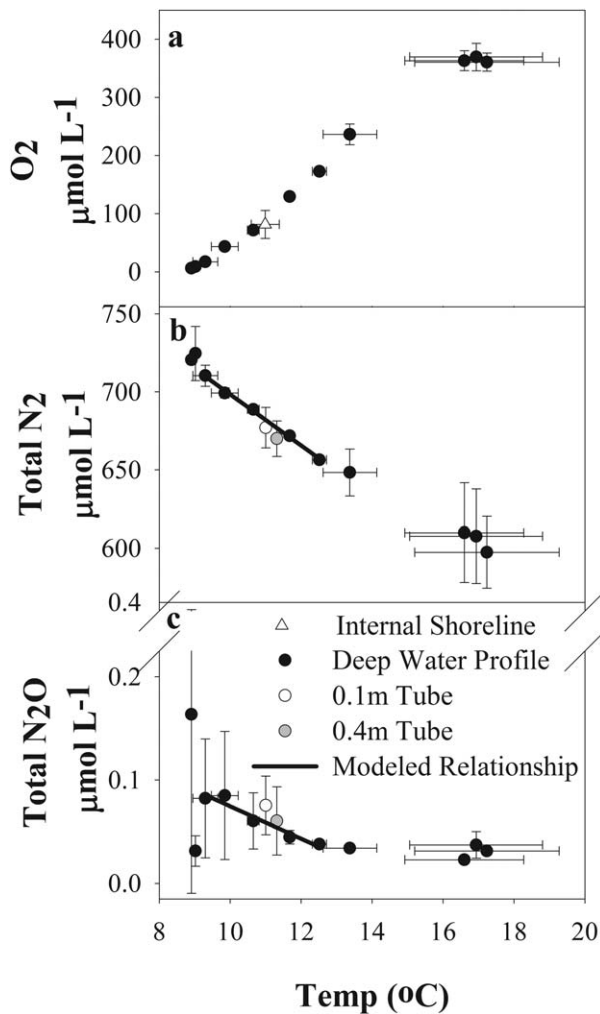
**Fig. 7.** Mean temperature plotted against mean $O_2$ (a), $N_2$ (b), and $N_2O$ (c) at 11 depths from the deep water site on 8 June 2012 and 19 June 2012 (black circles), and from the 23-h sampling event (white and gray circles). Internal shoreline $O_2$ concentration measurements were made by an optical $O_2$ probe at $z = 0.1$ m (white circle in panel a). Internal shoreline $N_2$ and $N_2O$ concentration measurements were made via tube sampling at 0.1m (white circles in panels b and c) and 0.4m (gray circles in panels b and c). Error bars represent 1 standard deviation from the mean.

6f). $N_2O$ averaged 0.08 $\mu$mol $N_2O$ L$^{-1}$ higher at 0.1 m off the bed than at 0.4 m off the bed (Std($G$) = 0.004 $\mu$mol $N_2O$ L$^{-1}$, $Z$-score = 1.93). All the significant concentration differences were observed following the arrival of the thin bore and prior to the collapse in stratification with the exception of one $N_2O$ set at 2:50 h on 16 June.

Internal shoreline $NO_3^-$ concentrations averaged 60.6 $\mu$mol L$^{-1}$ (SE $\pm$ 0.01 $\mu$mol L$^{-1}$, $n = 18$, Fig. 6d) and mean $NO_3^-$ concentration differences were below the instrument detection limit. $NH_4^+$ averaged 10.2 $\mu$mol L$^{-1}$ (Fig. 6d, SE. 1.0 $\mu$mol L$^{-1}$, $n = 18$), and the mean concentration difference was $-2.5$ $\mu$mol $NH_4^+$ (SE 1.4 $\mu$mol $NH_4^+$, $n = 9$) with

reduced near-bed concentrations of $NH_4^+$ ($C_1$-$C_2 < 0$) for seven out of nine grab samples.

**Sampling error**

Assuming a maximum temperature logger-related temperature gradient error of 0.008 °C, the average resulting artificial $N_2$ and $N_2O$ concentration differences are $\pm 0.1$ $\mu$mol $N_2$ L$^{-1}$ (or 2% of the mean concentration difference observed in this study) and undetectable, respectively. Variation in repeat sample measurements was quite high: 0.90% coefficient of variation for duplicate $N_2$ samples as compared to $\leq 0.3\%$ in other studies (Kana et al. 1994; Deemer et al. 2011) and 3.3% for duplicate $N_2O$ samples, which may have limited the ability to detect both $N_2$ and $N_2O$ concentration differences. For example, in the case where 0.1 m samples are overestimated and 0.4 m samples are underestimated, artificial concentration differences of 6.0 $\mu$mol $N_2$ L$^{-1}$ and 0.02 $\mu$mol $N_2O$ L$^{-1}$ could result. Finally, in addition to high coefficients of variation, discarded $O_2$ : Ar samples collected via tube-based sampling had approximately 40% higher calculated $O_2$ concentrations than those measured via the nearby optical probe. Permeability calculations, based on Fick's law, published values for the diffusion rates of gases in silicone rubber, and a direct test of diffusion rates in our sampling system suggest that at most 5.8 $\mu$mol $N_2$ L$^{-1}$ and 0.001 $\mu$mol $N_2O$ L$^{-1}$ could be lost from the samples during collection. Slightly more gas was likely lost from the 0.1 m tube (due to longer travel time and higher $N_2$ concentrations), such that diffusional loss would weaken observed concentration differences relative to actual field values. Hence, while sampling and analysis-associated uncertainty reduces the accuracy and precision of our analysis, errors generally would weaken observed concentration differences, but do not alter our fundamental insights and conclusions.

**Deep water profiles and modeling of lateral advection across the internal shoreline**

During the 23-h sampling event, temperatures and $O_2$ concentrations observed within the internal shoreline corresponded to a layer of water, approximately 4.5 m thick in the vertical direction, that was advected across the instrument deployment location. Based on the 8 June and 19 June deep-water profiles, internal shoreline temperatures and $O_2$ concentrations match those recorded between approximately 6.5 m and 11 m (Fig. 7a). Deep-water profiles also revealed factor of two differences in excess $N_2$, excess $N_2O$, and $NH_4^+$, but no large differences in the concentrations of $NO_3^-$ across this range of depths.

After correcting internal shoreline $N_2$ and $N_2O$ concentrations to reflect the permeability calculations (as described above), average concentrations of excess $N_2$ between 7 m and 9 m at the deep water site (24.6 $\mu$mol excess $N_2$ L$^{-1}$, SD 1.9, Fig. 7b) were significantly higher than within the internal shoreline (19.0 $\mu$mol $N_2$ L$^{-1}$, SD 9.3). Internal shoreline concentrations of excess $N_2O$ (0.6 $\mu$mol $N_2O$ L$^{-1}$, SD 0.03)

**Table 1.** Least squares linear regression $R^2$ and $p$ values for temperature-based modeling of dissolved solute concentrations between 5.5 m and 13 m at the deep water site on 19 June. All data met assumptions for equal variance and normal distribution. Regressions significant at $\alpha = 0.05$ are bolded

| Solute | Sign of correlation | $R^2$ | $p$ | Mean % error of modeled advection-based gradient |
|---|---|---|---|---|
| $N_2$ ($\mu$mol $L^{-1}$) | − | 1 | <0.001 | 2.3% |
| $N_2O$ ($\mu$mol $L^{-1}$) | − | 0.91 | 0.013 | 18.6% |
| $NH_4^+$ ($\mu$mol $L^{-1}$) | + | .006 | 0.903 | N.A. |
| $NO_3^-$ ($\mu$mol $L^{-1}$) | − | 0.246 | 0.395 | N.A. |

were not significantly different from concentrations between 7 m and 9 m at the deep water site (0.04 excess $\mu$mol $N_2O$ $L^{-1}$, SD 0.02, $n = 4$, Fig. 7c). This translates to higher observed $N_2O$ : $N_2$ ratios in the internal shoreline (0.0029) than at the deep water site (0.0016).

Temperature was strongly related to both $N_2$ and $N_2O$ concentrations at the deep water site, allowing for straightforward modeling of BBL concentration differences resulting from hypolimnion-wide $N_2$ and $N_2O$ accumulation ($R^2 > 0.9$, Table 1). Such "advection based" concentration differences in $N_2O$ and $N_2$ were larger than residual concentration differences. Averaged over the 23-h sampling period, residual concentration differences in both $N_2$ and $N_2O$ were not significantly different from zero. Residual $N_2O$ averaged 0.005 $\mu$mol $N_2O$ $L^{-1}$ higher at 0.1 m off the bed than at 0.4 m off the bed (Std(residual $G$) = 0.007, $Z$-score = 0.64) and 27 out of 37 residual $N_2O$ concentration differences were greater than 0. Residual $N_2$-N was an average of 1.4 $\mu$mol $N_2$ $L^{-1}$ higher at 0.1 m off the bed than at 0.4 m off the bed (Std(residual $G$) = 2.8, $Z$-score = 0.49), and 38 out of 74 residual $N_2$ concentration differences were bed-elevated. Error in residual concentration difference estimates may have resulted from uncertainty in the slope of the temperature vs. nitrogenous concentration regression lines that were used to model advection-based concentration differences. We calculated the standard error for this regression slope and propagated this error through Eq. 3. The resulting mean error was about 8% of the mean residual $N_2$ concentration difference ($\pm 0.1$ $\mu$mol $N_2$ $L^{-1}$) and 33% of the mean residual $N_2O$ concentration difference ($\pm 0.002$ $\mu$mol $N_2O$ $L^{-1}$). Detectable, statistically significant residual concentration differences in both solutes were observed after the arrival of the thin internal bore and before the collapse in BBL stratification. For $N_2$ a detectable residual concentration difference of 4.2 $\mu$mol $N_2$ $L^{-1}$ was observed on 15 June at 14:10 h (one sample $t$-test, $p < 0.5$, Fig. 6e). For $N_2O$ detectable residual concentration differences of 0.019 $\mu$mol $N_2O$ $L^{-1}$ and 0.015 $\mu$mol $N_2O$ $L^{-1}$ were observed on 15 Jun at 12:40 h and 17:30 h, respectively

(two sample $t$-test, $p < 0.05$, Fig. 6e,f). Significant residual $N_2$ concentration differences corresponded to the time of lowest $O_2$ concentrations within the BBL. Significant residual $N_2O$ concentration differences occurred both before and after the low $O_2$ period and corresponded to times of mid-range ambient $O_2$ within the BBL.

## Discussion

### Internal waves as drivers of boundary layer mixing

We report internal wave-induced fluctuations in both temperature and $O_2$ within the BBL of Lacamas' internal shoreline. Downslope flow was associated with slow prolonged increases in water temperature and oxygen whereas sudden decreases in temperature and oxygen often occurred during upslope flow (Fig. 3). These punctuated declines in BBL temperature and oxygen during upslope flow resulted from the arrival of internal bores. Some bores were particularly thin, extending < 0.4 m above the bed. For such bores, warmer more oxygenated water is maintained in the upper layers of the BBL resulting in the co-occurrence of strong stratification and upslope flow (Fig. 1d). This contrasts with the weak stratification during upslope flow that is expected (Fig. 1a) and often observed in Lacamas (Fig. 4) and other lakes (Lorke et al. 2005). Measurements of mixing are not presented here, but mixing may be enhanced by bores (Bluteau et al. 2011; Martini et al. 2013; Cossu and Wells 2014), or by the proximity of intense stratification to the bed, where turbulence is often relatively intense.

### Temperature-based modeling

The temperature-based modeling presented here identifies advection and mixing of lakewide stratification as a dominant driver of vertical differences in chemistry within the internal shoreline BBL. Thus, vertical differences in BBL chemistry were most intense when a thin bore enhanced BBL thermal stratification, whereas vertical differences in BBL chemistry collapsed when strongly sheared upslope flow eliminated thermal stratification (Fig. 6).

Despite the dominance of advection-induced concentration differences, the temperature-based modeling also captured potential hot moments for locally derived concentration differences during discrete portions of the wave cycle. Residual $N_2$ and $N_2O$ concentration differences were detectable following the arrival of the thin bore and prior to the collapse in BBL stratification (Fig. 6). Potential sources of the residual concentration differences include: (1) instantaneous production within the near-bed sediments, (2) in sediment convection, and (3) advection not represented by the temperature-based model used here.

Instantaneous production in near-bed sediments is consistent with the observed fluctuations in $O_2$ concentrations during the wave cycle. Correspondence between high biological $N_2$ concentration differences and low BBL $O_2$ concentrations is expected if gradients resulted from microbial

denitrification (compare Fig. 6c,e). In addition, significant biological $N_2O$ concentration differences occurred when $O_2$ concentrations were in the middle of the observed range (between 60 $\mu$mol $O_2$ $L^{-1}$ and 95 $\mu$mol $O_2$ $L^{-1}$). Although no $N_2O$ samples were collected when $O_2$ concentrations were at their lowest, rapid microbial $N_2O$ production under intermediate $O_2$ concentrations is consistent with the biochemistry of $N_2O$-producing microbes. Inefficient nitrification and denitrification are thought to occur at 60–95 $\mu$mol $O_2$ $L^{-1}$ because this represents the minimum oxygen threshold for nitrification and the maximum oxygen threshold for denitrification. $N_2O$ is a free intermediate in the denitrification pathway, and its reduction represents the final and least energy-efficient step of the process such that, at high $O_2$ concentrations, $N_2O$ reduction may be inhibited. Alternatively, nitrification can result in the production of $N_2O$ via the oxidation of the intermediate hydroxylamine or via the nitrifier-denitrifier pathway where organisms that oxidize ammonium to nitrate may also carry out the reduction of nitrate to $N_2O$ or $N_2$ (Wrage et al. 2001; Stein and Yung 2003). One study of ammonium-oxidizing bacteria (*Nitrosomonas* sp.) found that these organisms can produce up to 10% $N_2O$ under low oxygen conditions (Goreau et al. 1980). High BBL $NO_3^-$ concentrations (microbial populations favor the reduction of $NO_3^-$ over $N_2O$) are also consistent with active, sediment-based $N_2$ and $N_2O$ production (Fig. 6d).

In-sediment convection may also explain the residual concentration differences that formed following the arrival of the thin bore. Seiche-related pore water convection may occur when dense, cold water washes over warmer sediments and forces warmer pore water into the water column. Convection has potential to dramatically increase exchange of chemicals between sediments and the BBL (Kirillin et al. 2009). In our study, significant $N_2$ concentration differences immediately follow the arrival of cold water via upslope flow. While estimates of the timescale over which in-sediment convection is likely to occur are beyond the scope of our study, it is possible that convection caused a release of porewater $N_2$ into the water column.

Finally, physical advection and mixing could be responsible for the residual concentration differences measured during this study if the temperature-$N_2$ and temperature-$N_2O$ relationships used here did not successfully model such processes. In this case, the residual concentration differences measured within the internal shoreline would be an artifact of denitrification or $N_2O$ production elsewhere in the reservoir. The accuracy of advection modeling might be degraded by spatial heterogeneity in water chemistry and shorter timescale changes in solute concentrations. Observed velocities within the internal shoreline BBL suggest that water is advected about 600 m upslope and downslope during each wave cycle. Within this footprint, relationships between

temperature, $N_2$ and $N_2O$ may depart from the measured deep water values, particularly in relatively shallow locations.

### Internal shorelines as a potential denitrification hot spot

Despite the dynamic chemical environment within the internal shoreline, the effect of seiching on internal shoreline sediment microbial activity has rarely been studied and we are not aware of previous *in situ* studies. One recent mesocosm study compared three fully oxygenated sediment cores with three cores undergoing intermittent anoxic phases and found no statistical difference in the microbial activity or chemical composition between treatments (Frindte et al. 2013). However, this study did not mimic the physical wave dissipation or the fluctuations in temperature and chemicals (aside from oxygen) that occurs in situ during an internal wave cycle. Recently, disproportionately high rates of $N_2$ accumulation were observed within the anoxic metalimnion of an agriculturally influenced lake, especially under strong stratification (Grantz et al. 2012). Laboratory incubations revealed water-column $N_2$ accumulation, but metalimnion sediments were not incubated to assess their potential contribution (Grantz et al. 2012). Our analysis of vertical differences in chemistry within the internal shoreline of Lacamas is consistent with denitrification within internal shoreline sediments (Fig. 6e). We also document a peak in excess $N_2$ concentrations within the metalimnion of the lake (Fig. 2c), which may result, at least partially, from the advection of $N_2$ produced within the internal shoreline. While we did not observe large fluctuations in $NO_3^-$ concentration within the BBL, the large fluctuations in $NH_4^+$ and $O_2$ may support local production and subsequent consumption of oxidized N (Fig. 6c,d).

Although limited to just a few hours of significant residual differences in nitrogenous chemistry, these results suggest that further investigation of BBL gradients may prove fruitful, particularly if residual gradients can be combined with estimates of turbulent diffusivity to yield biogenic fluxes (Holtappels et al. 2011). Chemical fluxes on the continental shelf have been estimated from chemical gradients using turbulent diffusivity calculated from logarithmic boundary layer theory (McGillis et al. 2011). However, our measurements of order-one Richardson numbers indicate that mixing within 0.4 m of the bed was substantially inhibited by stratification, violating the assumptions of logarithmic boundary layer theory (Monin and Yaglom 1975). Alternative models for turbulent diffusivity would likely be required to accurately estimate fluxes in such a strongly stratified boundary layer.

As the internal shoreline represents a potentially significant areal extent and a potential hotspot for biogeochemical transformations, it merits additional study. The amplitude of internal waves in lakes is usually several meters, but can range up to 60 m (Van Senden and Imboden 1989). More

work is needed to understand the relative importance of this zone in system-wide denitrification and overall biogeochemical cycling. High temporal resolution, in situ approaches, such as the one described here, are likely to aid in understanding the dynamics of this region.

**Next steps**

Currently, in situ studies of aquatic denitrification rely on cumbersome measurements of gas transfer velocity or are limited to the lower water column of stratified lakes and reservoirs where $N_2$ can accumulate due to water-density gradients (Deemer et al. 2011; Grantz et al. 2012; Beaulieu et al. 2014). In principle, biogenic chemical fluxes can be estimated by combining the residual gradients investigated here with estimates of turbulent diffusivity (Holtappels et al. 2011; McGillis et al. 2011). The time series of vertical differences in BBL $N_2$ concentrations presented here is a first step toward the development of such a "flux gradient" approach to estimating dentrification and other important chemical fluxes. Flux gradient methods, which require only relatively easily measured mean concentrations (rather than the fast response measurements required for eddy covariance methods), have long been used in the atmospheric boundary layer (Högström 1996) and have recently been applied successfully to estimate mixing of $O_2$ in a marine BBL (McGillis et al. 2011). Currently, efforts are underway to improve sampling techniques and adapt the flux gradient approach to stratified conditions, for application to lakebed BBLs. The rapid variation in chemical gradients observed in this study argues for the continued development of techniques that can elucidate physically driven biogeochemical hot spots and hot moments at the sediment water interface.

## References

Beaulieu, J. J., R. L. Smolenski, C. T. Nietch, A. Townsend-Small, M. S. Elovitz, and J. P. Schubauer-Berigan. 2014. Denitrification alternates between a source and sink of nitrous oxide in the hypolimnion of a thermally stratified reservoir. Limnol. Oceanogr. **59**: 495–506. doi:10.4319/lo.2014.59.2.0495

Bluteau, C. E., N. L. Jones, and G. N. Ivey. 2011. Dynamics of a tidally-forced stratified shear flow on the continental slope. J. Geophys. Res.: Oceans **116**: C11017. doi:10.1029/2011JC007214

Bryant, L. D., C. Lorrai, D. F. McGinnis, A. Brand, A. Wüest, and J. C. Little. 2010. Variable sediment oxygen uptake in response to dynamic forcing. Limnol. Oceanogr. **55**: 950–964. doi:10.4319/lo.2010.55.2.0950

Cossu, R., and M. G. Wells. 2014. The interaction of large amplitude internal seiches with a shallow sloping lakebed: Observations of benthic turbulence in Lake Simcoe, Ontario, Canada. PLoS One **8**: e57444. doi:10.1371/journal.pone.0057444

David, M. B., L. G. Wall, T. V. Royer, and J. L. Tank. 2006. Denitrification and the nitrogen budget of a reservoir in an agricultural landscape. Ecol. Appl. **16**: 2177–2190. doi:10.1890/1051-0761(2006)016[2177:DATNBO]2.0.CO;2

Deemer, B. R., J. A. Harrison, and E. W. Whitling. 2011. Microbial dinitrogen and nitrous oxide production in a small eutrophic reservoir: An in situ approach to quantifying hypolimnetic process rates. Limnol. Oceanogr. **56**: 1189–1199. doi:10.4319/lo.2011.56.4.1189

Frindte, K., W. Eckert, K. Attermeyer, and H. P. Grossart. 2013. Internal wave-induced redox shifts affect biogeochemistry and microbial activity in sediments: A simulation experiment. Biogeochemistry **113**: 423–434. doi:10.1007/s10533-012-9769-1

Garrett, C., and B. Petrie. 1981. Dynamical aspects of the flow through the Strait of Belle Isle. J. Phys. Oceanogr. **11**: 376–393. doi:10.1175/1520-0485(1981)011<0376:DAOTFT>2.0.CO;2

Goreau, T. J., W. A. Kaplan, S. C. Wofsy, M. B. McElroy, F. W. Valois, and S. W. Watson. 1980. Production of $NO_2^-$ and $N_2O$ by nitrifying bacteria at reduced concentrations of oxygen. Appl. Environ. Microbiol. **40**: 526–532.

Grantz, E. M., A. Kogo, and J. T. Scott. 2012. Partitioning whole-lake DNF using in situ dinitrogen gas accumulation and intact sediment core experiments. Limnol. Oceanogr. **57**: 925–935. doi:10.4319/lo.2012.57.4.0925

Groffman, P. M., and others. 2006. Methods for measuring DNF: Diverse approaches to a difficult problem. Ecol. Appl. **16**: 2091–2122. doi:10.1890/1051-0761(2006)016[2091:MFMDDA]2.0.CO;2

Harrison, J. A., and P. A. Matson. 2003. Patterns and controls of nitrous oxide (N2O) emissions from drainage waters of the Yaqui Valley, Sonora, Mexico. Global Biogeochemical Cycles, **17**: (3), 1080, doi:10.1029/2002GB001991

Henderson, S. M., and B. R. Deemer. 2012. Vertical propagation of lakewide internal waves. Geophys. Res. Lett. **39**: L06405. doi:10.1029/2011GL050534

Högström, U. 1996. Review of some basic characteristics of the atmospheric surface layer. Boundary Layer Meteorol. **78**: 215-246. doi:10.1007/BF00120937

Holtappels, M., M. M. M. Kuypers, M. Schlüter, and V. Brüchert. 2011. Measurement and interpretation of solute concentration gradients in the benthic boundary layer. Limnol. Oceanogr.: Methods **9**: 1–13. doi:10.4319/lom.2010.9.1

Imberger, J. 1998. Flux paths in a stratified lake: A review, p. 1–17. *In* J. Imberger [ed.], Physical processes in lakes and oceans. American Geophysical Union.

Kana, T. M., C. Darkangelo, M. D. Hunt, J. B. Oldham, G. E. Bennett, and J. C. Cornwell. 1994. Membrane inlet mass spectrometer for rapid high-precision determination of $N_2$, $O_2$, and Ar in environmental water samples. Anal. Chem. **66**: 4166–4170. doi:10.1021/ac00095a009

Kirillin, G., C. Engelhardt, and S. Golosov. 2009. Transient convection in upper lake sediments produced by internal seiching. Geophys. Res. Lett. **36**: L18601. doi:10.1029/2009GL040064

Lohrmann, A., B. Hackett, and L. P. Røed. 1990. High resolution measurements of turbulence, velocity and stress using pulse-to-pulse coherent sonar. J. Atmos. Oceanic Technol. **7**: 19–37. doi:10.1175/1520-0426(1990)007<0019:HRMOTV>2.0.CO;2

Lombardi, C. M., and S. H. Hurlbert. 2009. Misprescription and misuse of one-tailed tests. Austral Ecol. **34**: 447–468. doi:10.1111/j.1442-9993.2009.01946.x

Lorke, A., B. Müller, M. Maerki, and A. Wüest. 2003. Breathing sediments: The control of diffusive transport across the sediment-water interface by periodic boundary-layer turbulence. Limnol. Oceanogr. **48**: 2077–2085. doi:10.4319/lo.2003.48.6.2077

Lorke, A., F. Peeters, and A. Wüest. 2005. Shear-induced convective mixing in bottom boundary layers on slopes. Limnol. Oceanogr. **50**: 1612–1619. doi:10.4319/lo.2005.50.5.1612/pdf

Martini, K. I., M. H. Alford, E. Kunze, S. M. Kelly, and J. D. Nash. 2013. Internal bores and breaking internal tides on the Oregon continental slope. J. Phys. Oceanogr. **43**: 120–139. doi:10.1175/JPO-D-12-030.1

McGillis, W. R., C. Langdon, B. Loose, K. K. Yates, and J. Corredor. 2011. Productivity of a coral reef using boundary layer and enclosure methods. Geophys. Res. Lett. **38**: L03611. doi:10.1029/2010GL046179

Monin, A. S., and A. M. Yaglom. 1975. Statistical fluid mechanics: Mechanics of turbulence. Dover.

Robb, W. L. 1968. Thin silicone membranes- their permeation properties and some applications. Ann. N. Y. Acad. Sci. **146**: 119–137. doi:10.1111/j.1749-6632.1968.tb20277.x

Rusello, P. J. 2009. A practical primer for pulse coherent instruments. Technical Report TN-027, 673 Nortek AS.

Ruxton, G. D., and M. Neuhäuser. 2010. When should we use one-tailed hypothesis testing? Methods Ecol. Evol. **1**: 114–117. doi:10.1111/j.2041-210X.2010.00014.x

Saunders, D. L., and J. Kalff. 2001. Denitrification rates in the sediments of Lake Memphremagog, Canada-USA. Water Res. **35**: 1897–1904. doi:10.1016/S0043-1354(00)00479-6

Seitzinger, S., and others. 2006. DNF across landscapes and waterscapes: A synthesis. Ecol. Appl. **16**: 2064–2090. doi:10.1890/1051-0761(2006)016[2064:DALAWA]2.0.CO;2

Stein, L. Y., and Y. L. Yung. 2003. Production, isotopic composition, and atmospheric fate of biologically produced nitrous oxide. Annu. Rev. Earth Planet Sci. **31**: 329–356. doi:10.1146/annurev.earth.31.110502.080901

Taylor, J. R. 1993. Turbulence and mixing in the boundary layer generated by shoaling internal waves. Dyn. Atmos. Oceans **19**: 233–258. doi:10.1016/0377-0265(93)90038-9

Thorpe, S. A. 1992. Thermal fronts caused by internal gravity waves reflecting from a slope. J. Phys. Oceanogr. **22**: 105–108. doi:10.1175/1520-0485(1992)022<0105:TFCBIG>2.0.CO;2

Thorpe, S. A. 1999. Fronts formed by obliquely reflecting internal waves at a sloping boundary. J. Phys. Oceanogr. **29**: 2462–2467. doi:10.1175/1520-0485(1999)029<2462:FFBORI>2.0.CO;2

Thorpe, S. A., and U. Lemmin. 1999. Internal waves and temperature fronts on slopes. Ann. Geophysicae **17**: 1227–1234. doi:10.1007/s00585-999-1227-6

Umlauf, L., and H. Burchard. 2011. Diapycnal transport and mixing efficiency in stratified boundary layers near sloping topography. J. Phys. Oceanogr. **41**: 329–345. doi:10.1175/2010JPO4438.1

Van Senden, D. C., and D. M. Imboden. 1989. Internal seiche pumping between sill-separated basins. Geophys. Astro. Fluid **48**: 135–150. doi:10.1080/03091928908219530

Walter, R. K., C. B. Woodson, P. R. Leary, and S. G. Monismith. 2014. Connecting wind-driven upwelling and offshore stratification to nearshore internal bores and oxygen variability. J. Geophys. Res.: Oceans **119**: 3517–3534. doi:10.1002/2014JC009998

Weiss, R. F. 1970. The solubility of nitrogen, oxygen and argon in water and seawater. Deep-Sea Res. **17**: 721–735. doi:10.1016/0011-7471(70)90037-9

Weiss, R. F., and B. A. Price 1980. Nitrous-oxide solubility in water and seawater. Mar. Chem. **8**: 347–359. doi:10.1016/0304-4203(80)90024-9

Winant, C. D. 1974. Internal surges in coastal waters. J. Geophys. Res. **79**: 4523–4526. doi:10.1029/JC079i030p04523

Wrage, N., G. L. Velthof, M. van Beusichem, and O. Oenema. 2011. Role of nitrifier denitrification in the production of nitrous oxide. Soil Biol. Biochem. **33**: 1723–1732. doi:10.1016/S0038-0717(01)00096-7